nature chemistry

ARTICLES

https://doi.org/10.1038/s41557-018-0011-1

Experimental and computational evidence of halogen bonds involving astatine

Ning Guo[1], Rémi Maurice[1], David Teze[1], Jérôme Graton[2], Julie Champion[1], Gilles Montavon[1]* and Nicolas Galland[2]*

The importance of halogen bonds—highly directional interactions between an electron-deficient σ-hole moiety in a halogenated compound and an acceptor such as a Lewis base—is being increasingly recognized in a wide variety of fields from biomedicinal chemistry to materials science. The heaviest halogens are known to form stronger halogen bonds, implying that if this trend continues down the periodic table, astatine should exhibit the highest halogen-bond donating ability. This may be mitigated, however, by the relativistic effects undergone by heavy elements, as illustrated by the metallic character of astatine. Here, the occurrence of halogen-bonding interactions involving astatine is experimentally evidenced. The complexation constants of astatine monoiodide with a series of organic ligands in cyclohexane solution were derived from distribution coefficient measurements and supported by relativistic quantum mechanical calculations. Taken together, the results show that astatine indeed behaves as a halogen-bond donor—a stronger one than iodine—owing to its much more electrophilic σ-hole.

The understanding, and in turn the control, of molecular interactions for the design of new molecules and materials with desired properties is of crucial interest for a wide community of chemists. Although already investigated in seminal works of the past century[1–5], halogen-bonding interactions have recently been recognized to play an important role in a variety of areas including crystal engineering, medicinal chemistry and organocatalysis[6–16]. According to the recent definition given by the International Union of Pure and Applied Chemistry (IUPAC), 'A halogen bond occurs when there is evidence of a net attractive interaction between an electrophilic region associated with a halogen atom in a molecular entity and a nucleophilic region in another, or the same, molecular entity'[17]. A typical feature of halogen-bonding interactions, denoted R–X···B, is the almost perfect linearity between the atom of the R group that is bound to X, the halogen atom itself and the nucleophilic site at the halogen-bond acceptor, B. The electrophilic region associated with a halogen atom in R–X is the so-called 'σ-hole'—a region with a positive molecular electrostatic potential centred on the R–X axis. This region can interact favourably with electron-rich sites, thus giving rise to halogen bonding[18].

The iodine, bromine, chlorine and to a lesser extent fluorine elements are known to be able to serve as halogen-bond (XB) donors[19], with a donating ability that increases with increasing polarizability, that is, F < Cl < Br < I. To characterize the XB acceptors, a halogen-bond basicity scale, pK_{BI2}, was proposed a few years ago[20]. This is identified 'as the thermodynamic tendency of a substance to act as a halogen-bond acceptor and measure this property by the equilibrium constants of halogen-bonding formation for a series of bases with a common reference acid, diiodine'. The interaction occurring between I_2 and a Lewis base in an alkane solvent is written as:

$$B + I_2 \rightleftharpoons B \cdots I\text{–}I$$

where I_2 is the considered Lewis acid, B is a Lewis base, and K_c is the related equilibrium constant. The pK_{BI2} values used to define the basicity scale with diiodine can thus be obtained as:

$$pK_{BI2} = \log K_c$$

Note that this basicity scale was validated for dihalogen and interhalogen compounds and that it is meant to be general[20]. Therefore, one may use it to compare the XB donor abilities of iodine and astatine.

Astatine ($Z = 85$), the heaviest naturally occurring halogen, has been recently identified as being of high potential interest for nuclear medicine applications[21,22]. Indeed, its 211 radioisotope exhibits physical properties that are remarkably suited for targeted alpha-immunotherapy (100% alpha emitter and a half-life of 7.2 h)[22–24]. Some clinical successes have been reported over the past decade[25–27], but the use of ^{211}At is currently hindered because little is known of the basic chemistry of astatine[21]. This challenge triggered new fundamental studies[28–33]. In light of its position in the periodic table, below iodine in the halogen group, and the fact that its polarizability was computed to be larger than that of iodine[34], one may expect astatine to be a stronger XB donor than iodine. Nevertheless, it has also been shown to have rather marked metallic properties[29,35,36], and the confirmation of astatine-based halogen bonds with experimental evidence is therefore important. In this work we have shown such interactions and have measured their strengths. However, astatine can only be produced in very small amounts and one can therefore only work at ultra-trace concentrations (typically below 1×10^{-10} M). This severely limits the available experimental techniques useful to study the nature and reactivity of astatine species (for example, no standard spectroscopic tool can be used at such low concentrations).

As shown in previous studies, competition methods can be used to study speciation changes with astatine and to determine the associated equilibrium constant[29–31,37]. The distribution coefficient D of astatine between two phases, that is the ratio of the astatine

[1]SUBATECH, UMR CNRS 6457, IN2P3/IMT Atlantique/Université de Nantes, Nantes, France. [2]CEISAM, UMR CNRS 6230, Université de Nantes, Nantes, France. *e-mail: montavon@subatech.in2p3.fr; nicolas.galland@univ-nantes.fr

radioactivity measured in an organic solution and the astatine radioactivity measured in an aqueous solution, is tracked while varying the initial concentrations of ligand(s). Modification of D suggests a change in speciation, and an increase in D shows a transfer of astatine species from the aqueous phase to the organic one. Modelling of the corresponding experimental data gives access to equilibrium constants. In this study, our objective was to highlight the complexation of an astatine species with different ligands in an alkane solvent (for possible comparison with the pK_{BI2} scale). We anticipate an influence of this phenomenon on the D distribution coefficient, which should enable the determination of the complexation constants. We selected the experimental conditions to ensure the occurrence of a single astatine species as XB donor in the organic phase, whereas in the aqueous phase others can be present. Among the dihalogen compounds involving astatine and potentially found in solution, namely AtCl, AtBr and AtI (refs [31,37]), only the AtI species fulfils these requirements. Therefore, halogen-bonding complexation is exclusively studied in this work with AtI as the halogen-bond donor. The potential ligands, that is, the halogen-bond acceptors, must be stable in the acidic and oxidizing conditions required to obtain AtI in solution. Hence, nine Lewis bases, stable enough under these experimental conditions and distributed over a wide range of basicity in the pK_{BI2} scale, were selected (see molecular structures below). Prior to the experimental and computational investigations of the halogen-bonded complexes, the similarities and differences of the AtI and I_2 XB donors were shown by means of quantum mechanical calculations.

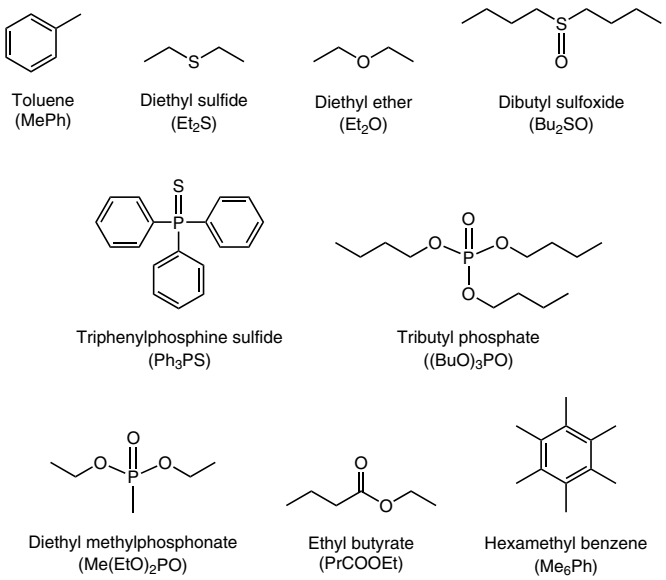

Results and discussion

Propensity to engage in halogen bonding for astatine versus iodine. Previous computational works have already indicated that astatine should behave as a strong XB donor, with different R groups bearing the At halogen (R = HO (ref. [38]), R = F, Cl, Br, I, At (ref. [39])). Here we investigate this further by taking into account the possibility that the least electronegative halogen may not necessarily be the halogen-bond donor, through a direct comparison between astatine and other halogens. Characterization of the donor abilities of At and I is based on the properties of both the monomeric and complexed XB donors. Relativistic effects, and especially spin–orbit coupling, may have a strong influence on the chemical bonds involving heavy atoms such as astatine[32,37,40–43], and are therefore included in our calculations. We selected the two-component relativistic density functional theory (DFT) approach that has previously proved to be reliable for studying a wide range of astatinated systems[37,41–44].

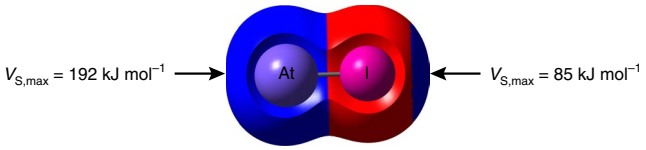

Fig. 1 | Side view of the molecular electrostatic potential for AtI calculated at the B3LYP/AVDZ level of theory. The molecular surface was defined by the isovalue of the electron density (0.001 e bohr^{-3}). Negative values are shown in red and positive values in blue.

As mentioned above, halogen bonding is intimately related to the concept of the σ-hole. The local maximum value ($V_{S,max}$) of the electrostatic potential at the molecular surface (molecular electrostatic potential, MEP) is a descriptor commonly used to characterize the halogen-bond donating ability of a given XB donor[6,45]. In the case of AtI, a positive region of the MEP is clearly observed on the astatine side (Fig. 1). On the opposite side of this molecule, the electron depletion related to the iodine σ-hole is much weaker. This strongly suggests that the astatine moiety is the most electrophilic region in AtI and that any halogen-bonding interaction should occur on this site.

Alternatively, computation of the strength of XBs involving either the astatine or the iodine atom is also a relevant descriptor to establish the preferred XB donor site in the AtI system. As mentioned above, we selected MePh, Me_6Ph, Et_2O and Et_2S Lewis bases (B) as halogen-bond acceptors for this purpose. At the B3LYP/AVDZ and PW6B95/AVDZ levels of theory, the halogen-bonded complexes involving the astatine site were systematically found to be stronger than those involving the iodine one, corroborating the higher XB donating ability of astatine compared to iodine. With Lewis bases Me_6Ph, Et_2O and Et_2S, the AtI···B structures were found to be at least 10 kJ mol^{-1} less stable than the IAt···B ones, implying negligible populations of complexes involving the iodine site. The lower free energy difference observed with MePh (4.2 kJ mol^{-1}, Supplementary Structures 2) still ensures that the IAt···B structures largely dominate the whole population of halogen-bonded complexes. Therefore, both investigated criteria lead us to the conclusion that, in AtI, astatine must be a stronger XB donor than iodine is, corroborating the conclusions of refs [38] and [39].

Experimental conditions to evidence XBs involving astatine. We selected the cyclohexane solvent because it is immiscible in water and was used to establish the pK_{BI2} scale. Here, we endeavour to determine the equilibrium constants of complexation between AtI and the B Lewis bases:

$$\overline{\mathrm{AtI}} + \overline{\mathrm{B}} \rightleftharpoons \overline{\mathrm{B \cdots AtI}} \qquad (1)$$

where the overlined notation indicates that these species belong to the organic phase. This equilibrium requires that AtI is present in the cyclohexane phase. To this end, the aqueous phase is prepared with 0.1 M of $HClO_4$. According to the Pourbaix (E–pH) diagram of astatine, At^+ is the main species present in the aqueous phase under these conditions (pH = 1.0 ± 0.2, E = 0.60 ± 0.04 V versus NHE)[29,30,44]. In the presence of I^- (0.01 or 0.1 M NaI), At^+ can form, in water, the AtI and AtI_2^- species with global equilibrium constants of $10^{6.1\pm0.2}$ and $10^{8.8\pm0.2}$, respectively[31]. In contrast to AtI_2^-, AtI is significantly extracted towards the organic phase and equilibrium (1) may therefore be established. Note that, as AtI, the At^+ species should initially be distributed between both phases[31,37]. The experimental conditions (Supplementary Fig. 1, [I^-] = 0.1 and 0.01 M) were therefore chosen such that the amount of At^+ was negligible and AtI was the only astatine species initially present in the organic phase, which should make the modelling of the experimental data more straightforward.

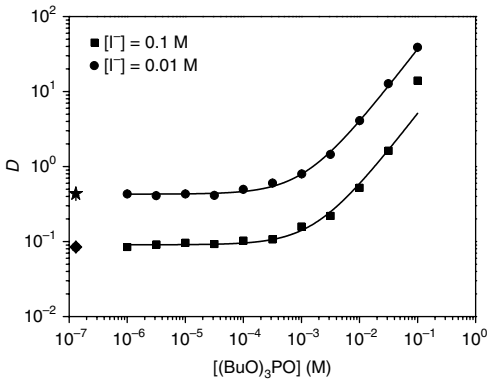

Fig. 2 | Distribution of astatine species between the organic and aqueous phases in the presence of $(BuO)_3PO$. Distribution coefficient *D* as a function of initial $(BuO)_3PO$ concentration in cyclohexane, with an aqueous phase initially containing 0.01 M (circles) and 0.1 M (squares) I^- (star and diamond indicate data without $(BuO)_3PO$). Model curves are displayed as solid lines. The increase in *D* shows a transfer of astatine species from the aqueous phase to the organic phase.

Table 1 | Equilibrium constants of AtI with different Lewis bases (B) obtained from the distribution coefficient measurements and from quantum mechanical calculations, and compared with pK_{BI2} values from the literature[20].

B	log K_{BAtI}			pK_{BI2}[20]
	Experiment[a]	B3LYP/AVDZ	PW6B95/AVDZ	
MePh	−0.67 (12)	−0.26	0.01	−0.44
PrCOOEt	0.46 (28)	1.26	1.00	0.04
Me_6Ph	0.67 (32)	0.50	1.36	0.14
$Me(EtO)_2PO$	1.75 (22)	-	-	1.57
Et_2O	1.53 (23)	0.61	0.66	−0.05
$(BuO)_3PO$	2.84 (13)	3.24	2.26	1.33
Bu_2SO	3.78 (20)	-	-	1.93
Ph_3PS	3.41 (38)	-	-	2.57
Et_2S	4.01 (31)	3.48	3.55	2.29

[a]For each Lewis base, one equilibrium constant can be obtained by fitting the experimental points corresponding to a given initial I^- concentration, the two values being used to compute an average K_{BAtI} value and the corresponding standard deviation is given in parenthesis.

Interaction of AtI with Lewis bases not extracted in the aqueous phase. We first focus on the Lewis bases that were found insoluble in water under the selected experimental conditions. Hence, complexation between AtI and the MePh, Me_6Ph, Et_2O, Et_2S, PrCOOEt, Ph_3PS and $(BuO)_3PO$ bases occurs solely in the organic phase and one assumes that the formed complexes remain in this phase. We thus expect to model the experimental data with a limited set of equilibrium reactions. Let us discuss the case of $(BuO)_3PO$ as an example. As anticipated, the astatine distribution coefficient is significantly influenced by the initial $(BuO)_3PO$ concentration. In Fig. 2, the two sets of experimental points, obtained with 0.1 M and 0.01 M I^-, respectively, behave in a 'parallel' way. The constant value of the distribution coefficient when the initial $(BuO)_3PO$ concentration is below 1×10^{-4} M suggests that no speciation change occurs in the organic phase and in the aqueous phase. In this concentration range, *D* is mainly governed by the extraction of AtI in cyclohexane. The value of *D* increases with the largest $(BuO)_3PO$ concentrations, indicating a competitive reaction that promotes transfer of astatine from water into the organic phase.

An appropriate modelling of *D* requires an inventory of the equilibria actually occurring in both phases. At first, reaction (2) rules the [AtI]/[AtI_2^-] ratio in the aqueous phase.[31]

$$AtI + I^- \rightleftharpoons AtI_2^- \qquad K = \frac{[AtI_2^-]}{[AtI]\,[I^-]} = 10^{2.7\pm0.3} \tag{2}$$

Two additional equilibria are then introduced to describe the extraction of the AtI species in cyclohexane and formation of the 1:1 halogen-bonded complexes (with overlined species relating to the organic phase):

$$AtI \rightleftharpoons \overline{AtI} \qquad D_1 = \frac{[\overline{AtI}]}{[AtI]} \tag{3}$$

$$\overline{AtI} + \overline{B} \rightleftharpoons \overline{B\cdots AtI} \qquad K_{BAtI} = \frac{[\overline{B\cdots AtI}]}{[\overline{AtI}]\,[\overline{B}]} \tag{4}$$

The astatine coefficient distribution *D* can finally be expressed from the concentrations of the ligand in the organic phase and of I^- in the aqueous phase:

$$D = \frac{D_1 + K_{BAtI}\times D_1\times[\overline{B}]}{1 + K\times[I^-]} \tag{5}$$

The value of D_1 is obtained at low Lewis base concentrations, in the range where *D* is found to be constant. On increasing the Lewis base concentration, the variation in *D* is then ruled by the K_{BAtI} parameter. Using equation (5), the two sets of experimental data can be satisfactorily and independently fitted (with D_1 and K_{BAtI} as adjustable parameters). For each initial I^- concentration (0.01 M or 0.1 M), the full run of experiments was performed twice, yielding one equilibrium constant value. The logarithm of the average K_{BAtI} value and the associated standard deviation are presented in Table 1 for $(BuO_3)PO$ and for the compounds analysed following the same protocol, MePh, Et_2O, PrCOOEt, Me_6Ph and Ph_3PS.

Among the Lewis bases that were found insoluble in the aqueous phase, Et_2S shows a distinct behaviour. With an initial 0.1 M concentration of I^- in the aqueous phase, *D* increases similarly to the formerly studied Lewis bases, and the fitted curve with the current model satisfactorily explains the data (dashed line in Fig. 3a). However, with an initial 0.01 M concentration of I^-, a plateau is observed with Et_2S concentrations larger than 1×10^{-3} M, after a sharp increase in the 1×10^{-5} to 1×10^{-3} M range. As shown in Fig. 3a, this behaviour cannot be reproduced with the model based on equation (5) (dotted line). Indeed, the astatine distribution coefficient is significantly overestimated by the initial model based on equation (5) at the highest concentrations of Et_2S (and the lowest concentration of I^-), which could be rationalized by the hypothesis that B···AtI or an additional astatine species is present in the aqueous phase. Because the former possibility is the most probable one under the experimental conditions, we here consider that B···AtI is extracted towards the aqueous phase according to equation (6):

$$B\cdots AtI \rightleftharpoons \overline{B\cdots AtI} \qquad D_2 = \frac{[\overline{BAtI}]}{[BAtI]} \tag{6}$$

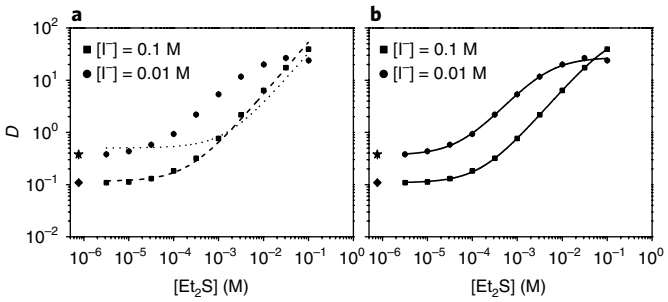

Fig. 3 | Distribution of astatine species between the organic and aqueous phases in the presence of Et_2S. Distribution coefficient D as a function of initial Et_2S concentration in cyclohexane, with an aqueous phase initially containing 0.01 M (circles) and 0.1 M (squares) I^- (star and diamond indicate data without Et_2S). **a**, Dashed and dotted lines correspond to the initial model (equation (5)). **b**, Solid lines correspond to the revised model (equation (7)). An increase in D shows a transfer of astatine species from the aqueous phase to the organic phase.

$$D = \frac{D_1 + K_{BAtI} \times D_1 \times [\overline{B}]}{1 + K \times [I^-] + K_{BAtI} \times D_1 \times [\overline{B}]/D_2} \quad (7)$$

The D_2 parameter is then introduced in a revised model (equation (7)) of the astatine distribution coefficient, convincingly fitting the whole set of experimental data (solid lines in Fig. 3b). Moreover, the K_{BAtI} values in the presence of 0.1 M NaI estimated from both equations (5) and (7) match reasonably. Therefore, we are confident that the log K_{BAtI} value of 4.01 obtained with the revised model is a reliable one.

Interaction of AtI with Lewis bases distributed between both aqueous and organic phases. $Me(EtO)_2PO$ and Bu_2SO are partly soluble in the aqueous phase. Their distribution coefficients (equation (8), $D_3 = 1 \times 10^{-0.57}$ and $1 \times 10^{-0.95}$, respectively) were determined from total organic carbon (TOC) measurements in the absence of astatine. Hence, the fitting model (equation (9)) has to take into account the partition of these Lewis bases between the aqueous and the organic phase.

$$B \rightleftharpoons \overline{B} \qquad D_3 = \frac{[\overline{B}]}{[B]} \quad (8)$$

$$D = \frac{D_1 + K_{BAtI} \times D_1 \times [\overline{B}] \times D_3/(D_3 + 2)}{1 + K \times [I^-]} \quad (9)$$

With Bu_2SO, the astatine distribution reveals a behaviour similar to those of many of the insoluble Lewis bases (Supplementary Fig. 2). The model based on equation (9) satisfactorily explains the experimental data. The same process was used to analyse those obtained with $Me(EtO)_2PO$. The K_{BAtI} values estimated with Bu_2SO and $Me(EtO)_2PO$ are reported in Table 1. Furthermore, the same values were obtained for K_{BAtI} if we consider that the B···AtI species are also present in the aqueous phase. This indicates that equation (6) has no relevancy to the K_{BAtI} determination, considering the chosen experimental conditions.

Comparison with the pK_{BI2} scale. An experimental but indirect proof that the interactions between AtI and the selected Lewis bases are indeed ruled by halogen bonding comes from a comparison between the measured equilibrium constants and the pK_{BI2} values.

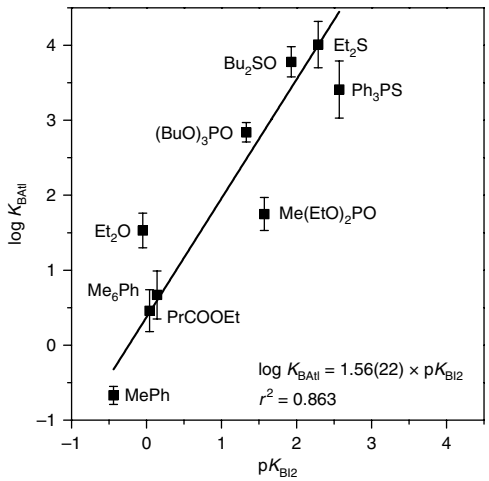

Fig. 4 | Relationship between XB equilibrium constants. The log K_{BAtI} values are derived from the astatine distribution coefficient D and pK_{BI2} values were measured via spectroscopic monitoring[20]. Error bars represent one standard deviation of uncertainty, and the standard deviation is computed from the two K_{BAtI} equilibrium constants obtained by fitting independently the two sets of experimental data (each corresponding to a given initial I^- concentration).

The pK_{BI2} values, extracted from the diiodine basicity scale of ref. [20], are reported in Table 1 for the experimental set of compounds, and Fig. 4 aims to correlate the log K_{BAtI} values to the pK_{BI2} ones. Overall, the log K_{BAtI} values increase with increasing pK_{BI2}. This indicates that (1) the interactions between AtI and these Lewis bases are similar to those observed with diiodine and (2) the basicity scale obtained with diiodine is indeed transferable to the AtI case. These are indirect proofs that the complexes implying AtI are ruled by halogen bonding. Furthermore, comparison of the complexation constants with those previously obtained with diiodine indicates that AtI interacts more strongly than I_2 with almost all the studied Lewis bases, suggesting that astatine should be the XB donor in AtI.

Comparison with DFT results. In a recent benchmark study focused on astatine compounds[43] it was shown that accurate equilibrium constants can be predicted with B3LYP and PW6B95 DFT functionals, used in conjunction with double zeta quality basis sets such as the AVDZ one, provided that isodesmic-like reactions (equation (10)) are considered in order to take advantage of error cancellation mechanisms:

$$B_1 \cdots AtI + B_2 \rightleftharpoons B_2 \cdots AtI + B_1 \quad (10)$$

When the complexation constant K_{B_1AtI} between AtI and the B_1 Lewis base is accurately known (from experiment), or its value is arbitrarily fixed, computation of the equilibrium constant K_{exc} of this exchange reaction (10) readily leads to the complexation constant of AtI with the B_2 Lewis base:

$$\log K_{B_2AtI} = \log K_{exc} + \log K_{B_1AtI} \quad (11)$$

Hence, it becomes possible to predict accurately the trend followed by AtI complexation constants within a series of Lewis bases. Note that a B···AtI species or a B Lewis base may exhibit several conformers; their free energies are in this case calculated according to a Boltzmann distribution. To model the experimental XB complexation with quantum mechanical calculations in a rather straightforward way, the theoretical investigations were limited to the

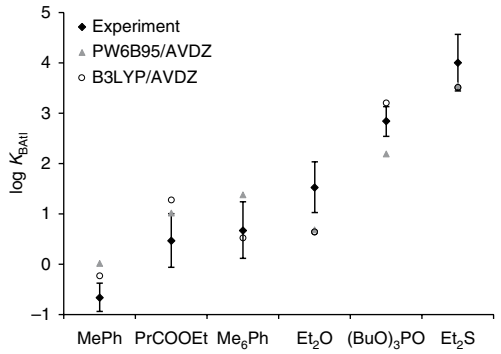

Fig. 5 | Compared evolutions of experimental and computational K_{BAtI} values for six XB acceptors. Error bars represent two standard deviations of uncertainty, and the standard deviation is computed from the two K_{BAtI} equilibrium constants obtained by fitting independently the two sets of experimental data (each corresponding to a given initial I^- concentration).

interactions between AtI and Lewis bases exclusively present in the organic phase (since solute–solvent interactions are weak in non-polar aprotic solvents such as cyclohexane, the presented results are only based on in vacuum calculations). The K_{BAtI} equilibrium constants computed at the B3LYP/AVDZ and PW6B95/AVDZ levels of theory, and translated according to the experimental values, are presented in Table 1. For each B···AtI system, the structure of the most stable conformer at the B3LYP/AVDZ level of theory is displayed in Supplementary Fig. 3. Whatever the studied B···AtI system, the interaction directly involves the At atom, the interaction distance is always lower than the sum of the van der Waals radii of involved atoms (2.02 Å for At (ref. [46])) and the formed angle is always close to 180°, which is in full agreement with the features expected for halogen-bonding interactions.

Having already established that the preferred halogen-bonding interaction site is the At atom in the AtI structure, it is important to check whether the theoretical predictions are consistent with our experimental results. Figure 5 (and similarly Supplementary Fig. 4) displays the trends followed by the calculated K_{BAtI} values, at the B3LYP/AVDZ and PW6B95/AVDZ levels of theory, for selected systems that span over the entire experimental scale. Although some individual constants are not perfectly reproduced, we feel that there is a satisfactory agreement with respect to the evolution of the measured equilibrium constants. The mean absolute deviation between experimental log K_{BAtI} values and the ones from B3LYP/AVDZ calculations is rather small, 0.54 in the unit of log (that is, 3.1 kJ mol^{-1} on the free energy scale) and the biggest discrepancy (0.9 units) is obtained with the Et_2O Lewis base. The mean absolute deviation is similar at the PW6B95/AVDZ level of theory (0.64 in the unit of log, that is, 3.6 kJ mol^{-1} on the free energy scale). Because both quantum mechanical calculations and experiments suggest, independently, that the B···AtI species are stabilized by astatine-mediated halogen bonds and, in light of the general agreement between theoretical and experimental results, we conclude that taken together the data points to experimental confirmation of astatine-based halogen bonds.

Conclusion

The complexation constants between AtI and a series of Lewis bases were obtained by analysing experimental data resulting from competition experiments. A trend similar to the XB basicity scale previously defined with diiodine was obtained, representing a first indirect indication of halogen bonding between AtI and the considered Lewis bases. This was further supported by relativistic quantum mechanical calculations. AtI was found to be a stronger halogen-bond donor than I_2. Furthermore, our theoretical study pointed to astatine bearing a more electrophilic site than iodine in AtI, and showed that the halogen-bonded complexes are systematically more stable when astatine rather than iodine acts as the XB donor. Taken together, these results confirm the full trend of halogen-bond donor characters as F < Cl < Br < I < At.

We hope that this work will trigger further research on halogen bonding and on astatine chemistry. In particular, it would be of great interest (1) to check if AtI can form 1:2 complexes, that is, At and I atoms being simultaneously involved in two different XB interactions; and (2) to design astatine compounds that are a stronger halogen-bond donor than AtI, to enlarge the XB acidity scale of astatine. Finally, the design of new ^{211}At-labelling reagents for targeted alpha-immunotherapy could take advantage of the propensity of astatine to form strong halogen bonds by strengthening the link between At-211 and the targeting agents, with the aim of hindering the deastatination phenomenon (the release of free astatide that occurs in vivo)[21,47]. It would also be interesting to investigate whether halogen bonding is also at play in previously reported studies[47,48].

Methods

Production of At-211. The At-211 used in this work was produced by the ARRONAX cyclotron in Nantes through the nuclear reaction ^{207}Bi(α, 2n)^{211}At. Bismuth-209 targets were irradiated for 2 h by alpha external beams accelerated at 28 MeV (ref. [49]). After irradiation of the target, a dry distillation method was used to isolate the At-211 and then recover 10 MBq of At-211 into 200 µl chloroform[50]. Then At-211 was back-extracted to a 0.1 M $HClO_4$ solution, conditions where the astatine species corresponds to At^+ (ref. [37]).

Analytic tools. The radioactivity in the two phases was measured with a Packard 2550 TR/AB Liquid Scintillation analyser with the Ultima Gold LLT scintillation liquid[37]. Quenching caused by the different solvents was considered to determine the At-211 activity (A) according to the following equation:

$$A = A_{mes} \times (8 \times 10^{-10} \times tSIE^3 - 2 \times 10^{-6} \times tSIE^2 + 0.0013 \times tSIE + 0.7228) \quad (12)$$

where A_{mes} is the activity measured by liquid scintillation and tSIE is the transformed spectral index of the external standard, a parameter defined by the apparatus for counting efficiency determination.

The possible solubility of the Lewis bases (B) in the aqueous phase was systematically checked with a TOC meter (Shimadzu TOC V CSH) in the absence of astatine. The distribution coefficient of B can be obtained by fitting the detected concentration in the aqueous phase as a function of the initial ligand concentration in cyclohexane.

An electrode (Inlab) freshly calibrated with standard pH buffers (pH 4.00 and 7.00, Merck) and a Pt combined redox electrode (Metrohm) calibrated with a redox buffer ($Fe(SCN)_6^{3-}$/$Fe(SCN)_6^{4-}$, 220 mV/Pt/SCE, Radiometer Analytical) were used to measure the pH and the potential E of the aqueous phase at equilibrium, respectively. No significant deviation from the targeted 1 and 0.6 V values, respectively, was observed.

Measurement of distribution coefficients. The liquid/liquid distribution of At-211 between an organic and an aqueous phase was determined with increasing amounts of initial Lewis bases concentrations in the organic phase. Note that no halogen bond is expected between AtI and the organic solvent, cyclohexane. The aqueous phase was composed of 0.1 M of $HClO_4$ with 0.01/0.1 M of NaI. Considering the pK_a value of HI (−9.5)[51], dissolved NaI salt initially produce 100% of the ionic species I^- given the experimental conditions. The systems were first equilibrated before the addition of At-211 (~1,000 Bq). After addition of astatine, 2 h of shaking was carried out to achieve distribution equilibrium of astatine between the two phases. Thus distribution coefficient D can be determined as

$$D = \frac{A_{org} \times V_{aq}}{A_{aq} \times V_{org}} \quad (13)$$

where V_{org} and V_{aq} are the given phase volumes and A_{org} and A_{aq} are the total astatine radioactivities in the organic and aqueous phases at equilibrium, respectively. Because the volume of the organic phase was taken as half that of the aqueous phase, equation (13) further simplifies to

$$D = \frac{2 \times A_{org}}{A_{aq}} \quad (14)$$

Therefore, it is easy to express back the activity in each phase in % of A_{tot}:

$$A_{org} = \frac{100D}{D+2} A_{tot}(\%) \quad (15)$$

and

$$A_{aq} = \frac{200}{D+2} A_{tot}(\%) \quad (16)$$

Modelling. The objective was to reproduce the experimental curves displaying D variations using parameters that are representative of the equilibria occurring (1) in the aqueous solution (for example, the complexation of AtI with I^-), (2) in the organic phase (for example, the interaction between AtI and the Lewis bases) and (3) between the two phases (for example, extraction of the various species). Once the appropriate equilibria were considered, an analytical expression was derived as a function of the different parameters. Origin 9.0 was used to fit the experimental data with this equation, to obtain the unknown parameters. The model is considered good when (1) it can well reproduce the experimental data with a minimum number of 'predictable' equilibria and (2) the fitting parameters are not strongly correlated.

Relativistic quantum mechanical calculations. Geometry optimizations and numerical frequency calculations were performed with the NWChem program, v. 5.1.1 (ref. [52]). The spin–orbit DFT (SODFT) method relying on relativistic pseudo-potentials was used, namely the small core ECP28MDF[53] and ECP60MDF[54] for I and At atoms, respectively. The hybrid B3LYP[55] and PW6B95[56] exchange-correlation functionals were selected as recommended in a recent benchmark study on astatine compounds[43]. Explicitly treated electrons were described using polarized double zeta basis sets, referred to as AVDZ, augmented with diffuse functions for non-hydrogen atoms[57–59] and supplemented with two-component extensions for astatine[37,54] and iodine[53,60] atoms. Interaction energies were corrected from the basis set superposition error using the counterpoise method[61]. Note that test calculations using the implicit solvation model recommended in ref. [43] have shown that the solvent effects, due to cyclohexane, are negligible on calculated equilibrium constants (for example, the log K_{BAtI} value for the AtI···Me_6Ph system is changed by 0.01 with respect to the one for AtI···Et_2O). Further calculations were performed to assess (1) the accuracy of the selected DFT functionals and basis sets and (2) the role of the relativistic spin–orbit interaction when halogen bonds involving astatine are studied. The results are presented in Supplementary Table 1.

Data availability. All data generated and analysed during this study are included in this Article and its Supplementary Information, and are also available from the authors upon reasonable request.

Received: 5 July 2017; Accepted: 18 January 2018;
Published online: 19 March 2018

References

1. Bent, H. A. Structural chemistry of donor–acceptor interactions. *Chem. Rev.* **68**, 587–648 (1968).
2. Desiraju, G. R. & Harlow, R. L. Cyano–halogen interactions and their role in the crystal structures of the 4-halobenzonitriles. *J. Am. Chem. Soc.* **111**, 6757–6764 (1989).
3. Amico, V., Meille, S. V., Corradi, E., Messina, M. T. & Resnati, G. Perfluorocarbon–hydrocarbon self-assembling. 1D infinite chain formation driven by nitrogen···iodine interactions. *J. Am. Chem. Soc.* **120**, 8261–8262 (1998).
4. Legon, A. C. π-Electron 'donor–acceptor' complexes B···ClF and the existence of the 'chlorine bond'. *Chem. Eur. J.* **4**, 1890–1897 (1998).
5. Valerio, G., Raos, G., Meille, S. V., Metrangolo, P. & Resnati, G. Halogen bonding in fluoroalkylhalides: a quantum chemical study of increasing fluorine substitution. *J. Phys. Chem. A* **104**, 1617–1620 (2000).
6. Cavallo, G. et al. The halogen bond. *Chem. Rev.* **116**, 2478–2601 (2016).
7. Li, B., Zang, S. Q., Wang, L. Y. & Mak, T. C. W. Halogen bonding: a powerful, emerging tool for constructing high-dimensional metal-containing supramolecular networks. *Coord. Chem. Rev.* **308**, 1–21 (2016).
8. Berger, G., Soubhye, J. & Meyer, F. Halogen bonding in polymer science from crystal engineering to functional supramolecular polymers and materials. *Polym. Chem.* **6**, 3559–3580 (2015).
9. Mukherjee, A., Tothadi, S. & Desiraju, G. R. Halogen bonds in crystal engineering: like hydrogen bonds yet different. *Acc. Chem. Res.* **47**, 2514–2524 (2014).
10. Breugst, M., Von Der Heiden, D. & Schmauck, J. Novel noncovalent interactions in catalysis: a focus on halogen, chalcogen, and anion-π bonding. *Synthesis* **49**, 3224–3236 (2017).
11. Nagorny, P. & Sun, Z. New approaches to organocatalysis based on C–H and C–X bonding for electrophilic substrate activation. *Beilstein J. Org. Chem.* **12**, 2834–2848 (2016).
12. Bulfield, D. & Huber, S. M. Halogen bonding in organic synthesis and organocatalysis. *Chem. Eur. J.* **22**, 14434–14450 (2016).
13. Wilcken, R., Zimmermann, M. O., Lange, A., Joerger, A. C. & Boeckler, F. M. Principles and applications of halogen bonding in medicinal chemistry and chemical biology. *J. Med. Chem.* **56**, 1363–1388 (2013).
14. Beale, T. M., Chudzinski, M. G., Sarwar, M. G. & Taylor, M. S. Halogen bonding in solution: thermodynamics and applications. *Chem. Soc. Rev.* **42**, 1667–1680 (2013).
15. Metrangolo, P. & Resnati, G. *Halogen Bonding I* (Springer, Berlin, 2015).
16. Metrangolo, P. & Resnati, G. *Halogen Bonding II* (Springer, Berlin, 2015).
17. Desiraju, G. R. et al. Definition of the halogen bond (IUPAC recommendations 2013). *Pure Appl. Chem.* **85**, 1711–1713 (2013).
18. Clark, T., Hennemann, M., Murray, J. S. & Politzer, P. Halogen bonding: the σ-hole. *J. Mol. Model.* **13**, 291–296 (2007).
19. Politzer, P., Lane, P., Concha, M. C., Ma, Y. & Murray, J. S. An overview of halogen bonding. *J. Mol. Model.* **13**, 305–311 (2007).
20. Laurence, C., Graton, J., Berthelot, M. & El Ghomari, M. J. The diiodine basicity scale: toward a general halogen-bond basicity scale. *Chem. Eur. J.* **17**, 10431–10444 (2011).
21. Wilbur, D. S. Enigmatic astatine. *Nat. Chem.* **5**, 246–246 (2013).
22. Vaidyanathan, G. & Zalutsky, M. R. Applications of ^{211}At and ^{223}Ra in targeted alpha-particle radiotherapy. *Curr. Radiopharm.* **4**, 283–294 (2011).
23. Vaidyanathan, G. & Zalutsky, M. R. Astatine radiopharmaceuticals: prospects and problems. *Curr. Radiopharm.* **1**, 177–196 (2008).
24. Guérard, F., Gestin, J.-F. & Brechbiel, M. W. Production of [^{211}At]-astatinated radiopharmaceuticals and applications in targeted α-particle therapy. *Cancer Biother. Radiopharm.* **28**, 1–20 (2013).
25. Zalutsky, M. R., Reardon, D. A., Pozzi, O. R., Vaidyanathan, G. & Bigner, D. D. Targeted α-particle radiotherapy with ^{211}At-labeled monoclonal antibodies. *Nucl. Med. Biol.* **34**, 779–785 (2007).
26. Zalutsky, M. & Reardon, D. Clinical experience with α-particle-emitting ^{211}At: treatment of recurrent brain tumor patients with ^{211}At-labeled chimeric antitenascin monoclonal antibody 81C6. *J. Nucl. Med.* **49**, 30–38 (2008).
27. Andersson, H. et al. Intraperitoneal α-particle radioimmunotherapy of ovarian cancer patients: pharmacokinetics and dosimetry of ^{211}At-MX$_{35}$ F(ab′)$_2$—a phase I study. *J. Nucl. Med.* **50**, 1153–1160 (2009).
28. Guérard, F., Lee, Y. S., Baidoo, K., Gestin, J. F. & Brechbiel, M. W. Unexpected behavior of the heaviest halogen astatine in the nucleophilic substitution of aryliodonium salts. *Chem. Eur. J.* **22**, 12332–12339 (2016).
29. Champion, J. et al. Astatine standard redox potentials and speciation in acidic medium. *J. Phys. Chem. A* **114**, 576–582 (2010).
30. Sergentu, D. C. et al. Advances on the determination of the astatine Pourbaix diagram: predomination of $AtO(OH)_2^-$ over At^- in basic conditions. *Chem. Eur. J.* **22**, 2964–2971 (2016).
31. Guo, N. et al. The heaviest possible ternary trihalogen species, $IAtBr^-$, evidenced in aqueous solution: an experimental performance driven by computations. *Angew. Chem. Int. Ed.* **128**, 15595–15598 (2016).
32. Pilme, J. et al. QTAIM analysis in the context of quasirelativistic quantum calculations. *J. Chem. Theory Comput.* **10**, 4830–4841 (2014).
33. Rothe, S. et al. Measurement of the first ionization potential of astatine by laser ionization spectroscopy. *Nat. Commun.* **4**, 1835 (2013).
34. Fleig, T. & Sadlej, A. J. Electric dipole polarizabilities of the halogen atoms in $^2P_{1/2}$ and $^2P_{3/2}$ states: scalar relativistic and two-component configuration–interaction calculations. *Phys. Rev. A* **65**, 032506 (2002).
35. Corson, D. R., MacKenzie, K. R. & Segre, E. Artificially radioactive element 85. *Phys. Rev.* **58**, 672 (1940).
36. Hermann, A., Hoffmann, R. & Ashcroft, N. W. Condensed astatine: monatomic and metallic. *Phys. Rev. Lett.* **111**, 116404 (2013).
37. Champion, J. et al. Assessment of an effective quasirelativistic methodology designed to study astatine chemistry in aqueous solution. *Phys. Chem. Chem. Phys.* **13**, 14984–14992 (2011).
38. Alkorta, I., Blanco, F., Solimannejad, M. & Elguero, J. Competition of hydrogen bonds and halogen bonds in complexes of hypohalous acids with nitrogenated bases. *J. Phys. Chem. A* **112**, 10856–10863 (2008).
39. Hill, J. G. & Hu, X. Theoretical insights into the nature of halogen bonding in prereactive complexes. *Chem. Eur. J.* **19**, 3620–3628 (2013).
40. Maurice, R. et al. Effective bond orders from two-step spin–orbit coupling approaches: the I_2, At_2, IO^+, and AtO^+ case studies. *J. Chem. Phys.* **142**, 094305 (2015).
41. Pilmé, J., Renault, E., Ayed, T., Montavon, G. & Galland, N. Introducing the ELF topological analysis in the field of quasirelativistic quantum calculations. *J. Chem. Theory Comput.* **8**, 2985–2990 (2012).
42. Sergentu, D., Amaouch, M., Pilmé, J., Galland, N. & Maurice, R. Electronic structures and geometries of the XF_3 (X=Cl, Br, I, At) fluorides. *J. Chem. Phys.* **143**, 114306 (2015).
43. Sergentu, D.-C., David, G., Montavon, G., Maurice, R. & Galland, N. Scrutinizing 'invisible' astatine: a challenge for modern density functionals. *J. Comput. Chem.* **37**, 1345–1354 (2016).

44. Champion, J. et al. Investigation of astatine(III) hydrolyzed species: experiments and relativistic calculations. *J. Phys. Chem. A* **117**, 1983–1990 (2013).
45. Kolář, M. H. & Hobza, P. Computer modeling of halogen bonds and other σ-hole interactions. *Chem. Rev.* **116**, 5155–5187 (2016).
46. Mantina, M., Chamberlin, A. C., Valero, R., Cramer, C. J. & Truhlar, D. G. Consistent van der Waals radii for the whole main group. *J. Phys. Chem. A* **113**, 5806–5812 (2009).
47. Wilbur, D. S. et al. Reagents for astatination of biomolecules: comparison of the in vivo distribution and stability of some radioiodinated/astatinated benzamidyl and nido-carboranyl compounds. *Bioconjug. Chem.* **15**, 203–223 (2004).
48. Makvandi, M. et al. The pre-clinical characterization of an alpha-emitting sigma-2 receptor targeted radiotherapeutic. *Nucl. Med. Biol.* **43**, 35–41 (2016).
49. Alliot, C., Cherel, M., Barbet, J., Sauvage, T. & Montavon, G. Extraction of astatine-211 in diisopropylether (DIPE). *Radiochim. Acta* **97**, 161–165 (2009).
50. Lindegren, S., Bäck, T. & Jensen, H. J. Dry-distillation of astatine-211 from irradiated bismuth targets: a time-saving procedure with high recovery yields. *Appl. Radiat. Isot.* **55**, 157–160 (2001).
51. Trummal, A., Lipping, L., Kaljurand, I., Koppel, I. A. & Leito, I. Acidity of strong acids in water and dimethyl sulfoxide. *J. Phys. Chem. A* **120**, 3663–3669 (2016).
52. Straatsma, T. P. et al. *NWChem, A Computational Chemistry Package for Parallel Computers* v.5.1.1 (Pacific Northwest National Laboratory, Richland, 2008).
53. Peterson, K. A., Shepler, B. C., Figgen, D. & Stoll, H. On the spectroscopic and thermochemical properties of ClO, BrO, IO, and their anions. *J. Phys. Chem. A* **110**, 13877–13883 (2006).
54. Peterson, K. A., Figgen, D., Goll, E., Stoll, H. & Dolg, M. Systematically convergent basis sets with relativistic pseudopotentials. II. Small-core pseudopotentials and correlation consistent basis sets for the post-*d* group 16–18 elements. *J. Chem. Phys.* **119**, 11113–11123 (2003).
55. Stephens, P. J., Devlin, F. J., Chabalowski, C. F. & Frisch, M. J. Ab initio calculation of vibrational absorption and circular dichroism spectra using density functional force fields. *J. Phys. Chem.* **98**, 11623–11627 (1994).
56. Zhao, Y. & Truhlar, D. G. Design of density functionals that are broadly accurate for thermochemistry, thermochemical kinetics, and nonbonded interactions. *J. Phys. Chem. A* **109**, 5656–5667 (2005).
57. Dunning, J., Peterson, K. A. & Wilson, A. K. Gaussian basis sets for use in correlated molecular calculations. X. The atoms aluminum through argon revisited. *J. Chem. Phys.* **114**, 9244–9253 (2001).
58. Dunning, T. H. Jr Gaussian basis sets for use in correlated molecular calculations. I. The atoms boron through neon and hydrogen. *J. Chem. Phys.* **90**, 1007 (1989).
59. Kendall, R. A., Dunning, T. H. Jr & Harrison, R. J. Electron affinities of the first-row atoms revisited. Systematic basis sets and wave functions. *J. Chem. Phys.* **96**, 6796 (1992).
60. Armbruster, M. K., Klopper, W. & Weigend, F. Basis-set extensions for two-component spin–orbit treatments of heavy elements. *Phys. Chem. Chem. Phys.* **8**, 4862–4865 (2006).
61. Boys, S. & Bernardi, F. The calculation of small molecular interactions by the differences of separate total energies. Some procedures with reduced errors. *Mol. Phys.* **19**, 553–566 (1970).

Acknowledgements

This work was supported in part by grants from the French National Agency for Research called 'Investissements d'Avenir' (ANR-11-EQPX-0004, ANR-11-LABX-0018). The work was carried out using HPC resources from GENCI-CINES/IDRIS (grant 2016-x2016085117) and from CCIPL (Centre de Calcul Intensif des Pays de la Loire). The authors acknowledge the GIP ARRONAX for the production of At-211.

Author contributions

N.Guo, J.C., D.T., J.G., R.M. and G.M. conceived and performed the experimental study. D.T., R.M., J.G. and N.Galland conceived and performed the computational studies. All authors jointly discussed the results and their interpretation, and participated in writing the manuscript.

Competing interests

The authors declare no competing interests.

Additional information

Supplementary information is available for this paper at https://doi.org/10.1038/s41557-018-0011-1.

Reprints and permissions information is available at www.nature.com/reprints.

Correspondence and requests for materials should be addressed to G.M. or N.G.

Publisher's note: Springer Nature remains neutral with regard to jurisdictional claims in published maps and institutional affiliations.